

# Application of Directional Thermal Conductivity to the Melt Region of the Reactor Lower Head during a Severe Accident

Kukhee Lim\*, Yong Jin Cho, Eunho Kim, Dongju Jang  
Korea Institute of Nuclear Safety, Gwahak-ro 62, Daejeon, Republic of Korea, 34142  
\*Corresponding author: limkh@kins.re.kr

\***Keywords** : severe accident, ablation of reactor lower head, anisotropic thermal conductivity, finite element analysis

## 1. Introduction

To assess the effectiveness of the in-vessel retention strategy during a severe accident and the timing of the reactor lower head failure, a comprehensive understanding of the lower head failure mechanism is essential. In particular, the timing of the reactor lower head failure is a critical factor in determining the progression of ex-vessel severe accident phenomena. From this point of view, the IVMR project WP2.4 [1] evaluated the feasibility of applying the in-vessel melt retention (IVR) strategy to VVER-1000 and next-generation reactors by analyzing reactor pressure Vessel (RPV) failures at different pressures. The result indicates that failure did not occur at low pressures (3 bar) but was observed at high pressures (40-52 bar).

Building on previous IVMR studies, a new IAEA CRP [2] benchmark was established, incorporating realistic thermal and mechanical loads for the VVER-1000 reactor. Finite Element Analysis (FEA) was employed to evaluate heat transfer, focusing on heat flux application and thermal conductivity adjustments. Thermal and mechanical loads were applied sequentially, with the inner wall experiencing high heat flux while the outer wall remained cooled. To simulate local melting, thermal conductivity was increased rather than employing element killing. However, multidirectional heat transfer within melt region can reduce the heat flux reaching the melt front, potentially overestimating remaining wall thickness. Therefore, this study investigates the effect of heat transfer directionality in the melt region to improve the accuracy of remaining wall thickness prediction.

## 2. Modeling

### 2.1 Geometry and Loading Conditions

The benchmark problem used in this study is based on the lower head of the VVER-1000 reactor. The coordinates of the inner and outer wall nodes were defined, and the lower head was divided into multiple segments. Each segment was assigned heat flux at in-vessel wall and temperature loads at ex-vessel wall according to the benchmark specifications. The inner wall experiences high heat flux, while the outer wall remains cooled at a lower temperature. The heat flux and temperature loads change over time, with the

maximum heat flux occurring at 7599 seconds. The highest recorded heat flux was 802,817.6 W/m<sup>2</sup> at segment 21 in Fig. 1. Fig. 2 shows heat flux input at inner wall.

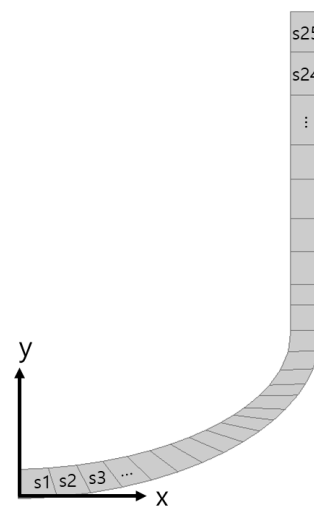


Fig. 1. Benchmark problem shape and segmentation

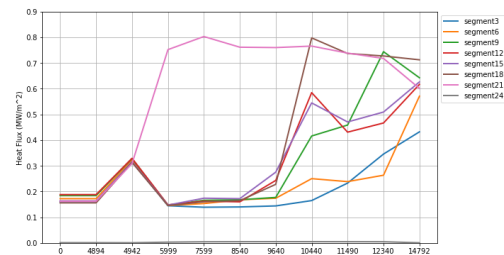


Fig. 2. Heat flux at the inner wall

In this study, only heat transfer analysis was performed, excluding pressure and gravity effects from relocated core materials. This allows for a more accurate evaluation of the thermal behavior of the lower head under severe accident conditions.

### 2.2 Material Properties

In this study, the thermal properties of two RPV materials were compared: 15X2HMΦA [3], a low-alloy steel used in the Russian VVER-1000 reactor, and SA533B1 [4], a low-alloy steel commonly used in U.S. reactor vessels (see Fig. 3-6). In the case of 15X2HMΦA, since the analysis is required up to the

melting point, the value at the highest temperature in the provided range has been extended to the melting point in the same manner in the high temperature range where the properties are not provided. The two materials show differences in temperature resolution, exhibiting abrupt changes at 750°C due to a ferrite-to-austenite phase transformation in the case of SA533B1. The variation in specific heat leads to differences in thermal diffusivity, despite both materials having similar thermal conductivity near the melting point.

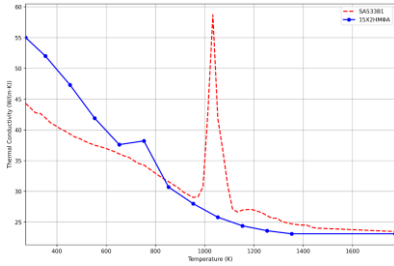


Fig. 3. Comparison of thermal conductivity

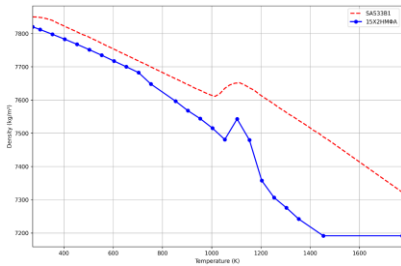


Fig. 4. Comparison of density

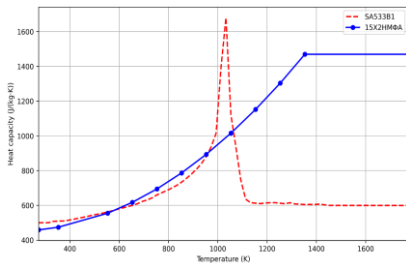


Fig. 5. Comparison of specific heat

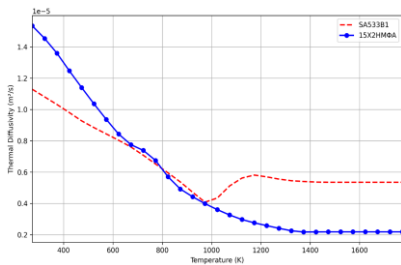


Fig. 6. Comparison of thermal diffusivity

According to the latest OECD/NEA technical report on reactor pressure vessel integrity assessment for IVR applications [5], the thermal properties of 15X2HMΦA appear to be similar to those of SA533B1 as shown in Fig. 7. The report indicates that the specific heat of 15X2HMΦA shows no significant difference from

SA533B1, and the specific heat values provided by the benchmark appear to follow Eq. 1 [6].

$$c_p [J/(kg \cdot K)] = 482.2 - 0.29797T + 0.7404 \cdot 10^{-3}T^2 \quad \text{Eq. 1}$$

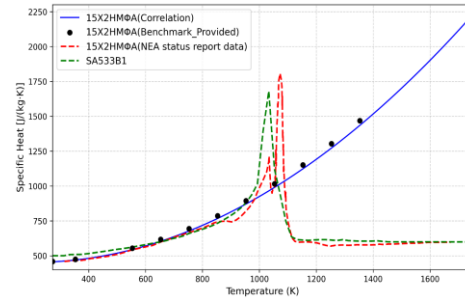


Fig. 7. Review of specific heat of 15X2HMΦA

### 2.3 Finite Element Modeling

The finite element analysis in this study was conducted using ANSYS Mechanical 2023 R1 [7]. The geometry was modeled as a two-dimensional axisymmetric representation using PLANE292, a four-node element designed for thermal conduction analysis. The mesh size was set to  $5 \times 10^{-3}$  m in ANSYS Workbench to allow automatic mesh generation, resulting in a total of 40,113 elements. The primary variable considered in the analysis was the melting phenomenon. Rather than removing finite elements and altering the analysis domain, melting was modeled by adjusting the thermal conductivity to minimize heat transfer within the molten region. This approach ensures numerical stability while accurately representing the heat transfer behavior in the reactor pressure vessel under severe accident conditions.

## 3. Analysis

### 3.1 Definition of the analysis cases

To prevent temperature of elements in the melt region from exceeding the melting point and to ensure direct heat transfer to the melt front, thermal conductivity was significantly increased above the melting point. However, discussions during the benchmarking highlighted a potential problem: when isotropic thermal conductivity is applied, heat flux may not transfer directly to the melt front, but dispersed in multiple directions, distorting the expected magnitude of heat flux at the melt front. To address this, the present study considers thermal conductivity control as a key parameter in modeling the melting phenomenon and controlling heat transfer direction at the melt front. In addition, the effect of material property differences between 15X2HMΦA and SA533B1, as discussed in Chapter 2, was included as a variable in analysis. Based on these considerations, the analysis cases were defined in Table 1.

Table I: Analysis Cases

No. of case	Material (15X2HMΦA, SA533B1)	Thermal conductivity for melt region (O, X)*	Thermal conductivity Directionality
1	SA533B1	X	isotropic
2	15X2HMΦA	X	isotropic
3	SA533B1	O	isotropic
4	15X2HMΦA	O	isotropic
5	SA533B1	O	anisotropic
6	15X2HMΦA	O	anisotropic

\*O: using high thermal conductivity in melt region  
X: using thermal conductivity at melting point

### 3.2 Results

#### A. Effect of melt region modeling

The results of cases 1 to 4 were compared to investigate the effect of melt region modeling. Figures 8-11 show the temperature distribution depending on the material difference and whether the temperature distribution above the melting point is included.

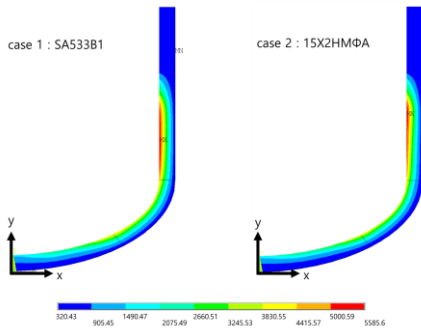


Fig. 8. Temperature of case 1 and 2 (unit: K, full range of temperature)

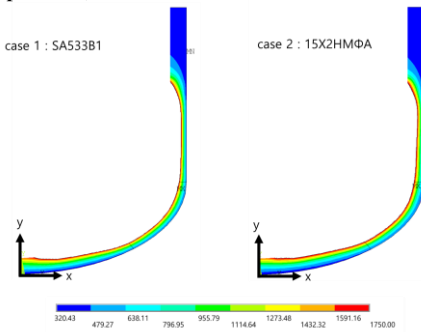


Fig. 9. Temperature of case 1 and 2 (unit: K, temperature range below the melting point)

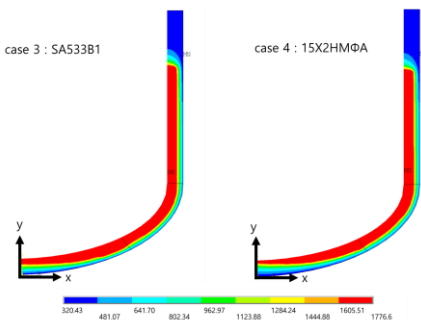


Fig. 10. Temperature of case 3 and 4 (unit: K, full range of temperature)

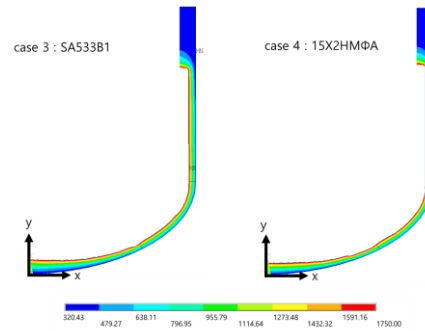


Fig. 11. Temperature of case 3 and 4 (unit: K, temperature range below the melting point)

At the end of the analysis ( $t = 14792$  s), temperature distribution shows no significant material-based difference. Figures 9 and 11 show thickness profiles differ depending on thermal conductivity adjustments in the melt region. While the remaining thickness at the location of maximum heat flux (around segment 21) is similar across all cases, melting is significantly less pronounced at low inclination angles in cases 1 and 2. This is because cases 1 and 2 require a significant amount of heat to raise the temperature of the melt, resulting in a lower total melt volume compared to cases 3 and 4. However, as shown in Fig. 12, in the region of maximum heat flux, the heat transferred to the sidewall is relatively greater due to the high thermal conductivity set in all directions at temperatures above the melting point in cases 3 and 4, so the heat flux in the thickness direction at melt front is lower as shown in Fig. 13.

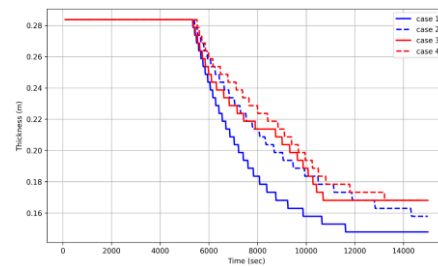


Fig. 12. Remained thickness by melting (at segment 21, case 1-4)

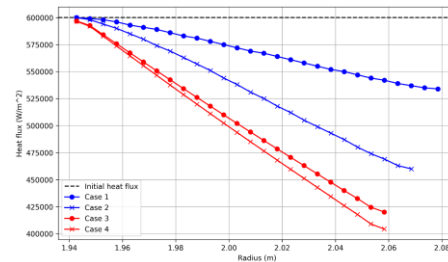


Fig. 13. Heat flux through thickness direction (at segment 21, case 1-4,  $t = 14792$  s)

### B. Effect of thermal conductivity directionality

As observed in Fig. 13, when the thermal conductivity is set to be isotropically high above the melting point, the heat flux reaching the melt front is reduced compared to the initial input. However, in cases 5 and 6, where the thermal conductivity is set to be anisotropic (increasing only in the thickness direction), this reduction in heat flux is mitigated. The temperature distribution shown in Fig. 14 shows no significant difference between the two materials. However, Fig. 15 shows that when anisotropic thermal conductivity is considered in cases 5 and 6, the wall thickness is approximately 4 cm thinner than in cases 3 and 4. Although the rate of material removal differs between the materials, the final wall thickness remains the same due to the identical thermal conductivity values above the melting point, despite the differences in thermal diffusivity. In addition, a direct comparison of heat flux in Fig. 16 shows that cases 3 and 4 experience a significantly greater reduction in heat flux compared to cases 5 and 6.

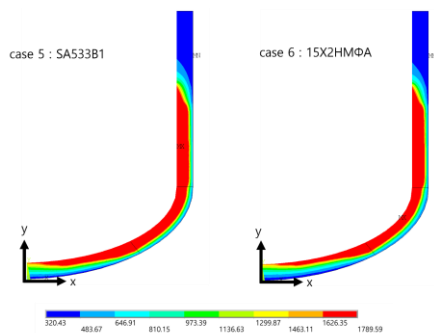


Fig. 14. Temperature of case 5 and 6 (unit: K, full range of temperature)

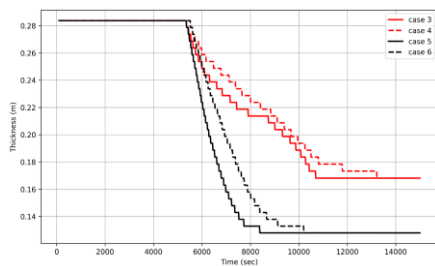


Fig. 15. Remained thickness by melting (at segment 21, case 3-6)

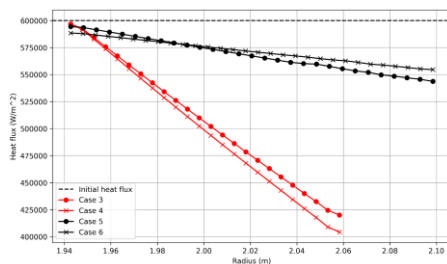


Fig. 16. Heat flux through thickness direction (at segment 21, case 3-6,  $t = 14792$  s)

## 4. Conclusions

This study investigated the IAEA CRP benchmark problem, analyzing the structural integrity of the VVER-1000 reactor lower head under external reactor vessel cooling. The analysis originally included heat transfer and structural analysis, but in this study the focus was on heat transfer and a method for applying the heat flux boundary condition at the melt front. If the thermal conductivity of the melt is not controlled, the melt region acts as a virtual heat sink, reducing the heat transfer to the wall. To eliminate this effect, the thermal conductivity was increased above the melting point to ensure direct heat transfer to the melt front. Isotropic thermal conductivity resulted in a higher heat flux to the sidewall, reducing the heat flux to the melt front. To avoid this, anisotropic thermal conductivity was applied, making the thermal conductivity high only in the direction of the wall thickness. This minimized heat flux reduction to the melt front, while the remaining wall thickness was further reduced.

## Acknowledgements

This work was supported by the Nuclear Safety Research Program through the Korea Foundation Of Nuclear Safety (KoFONS) using financial resources granted by the Nuclear Safety and Security Commission (NSSC) of the Republic of Korea (No. 2106007).

## REFERENCES

- [1] W. Villanueva, A. Filippov, S. Jules, K. Lim, M. Jobst, A. Bouydo, S. Qais, H. Wang, F. Fichot, and S. Bechta, Thermo-mechanical modelling of reactor pressure vessel during core melt in-vessel retention, International Seminar “In-vessel retention: Outcomes of IVMR project,” Palais des Congrès, Juan-les-Pins, France, Jan. 21-23, 2020.
- [2] International Atomic Energy Agency (IAEA), Developing a Phenomena Identification and Ranking Table, and a Validation Matrix, and Performing a Benchmark for In-Vessel Melt Retention – Final Report of a Coordinated Research Project, IAEA TECDOC-#####, 2025 (planned).
- [3] W. Villanueva and H. Wang, VVER-1000 Mechanical FEA benchmark, internal document for the IAEA CRP, Royal Institute of Technology (KTH), 2023.
- [4] J. E. Daw, J. L. Rempe, and D. L. Knudson, Thermal properties of structural materials used in LWR vessels, Journal of Nuclear Materials, Vol. 401, No. 1–3, pp. 65-70, 2010.
- [5] OECD/NEA, Status report on the reactor pressure vessel integrity assessment for in-vessel retention, Working Group on Integrity and Ageing of Components and Structures (WGIAGE) and Working Group on Analysis and Management of Accidents (WGAMA), 2025.
- [6] P. Gál, D. Gabriel, and P. Dymáček, Private correspondence from Nov. 16: Results of project TITSSUJB938 “A method to estimate integrity of nuclear reactor pressure vessel in severe accident with core melting,” UJV Řež, a. s., 2022.
- [7] ANSYS, ANSYS Mechanical User’s Guide, Release 2023 R1, ANSYS Inc., 2023.